Journal Pre-proofs

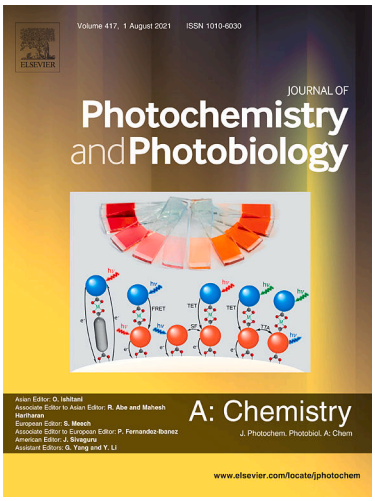

TiO_2-C nanocomposite synthesized via facile surfactant-assisted method as a part of less energy-consuming LED-based photocatalytic system for environmental applications

Adam Kubiak, Anna Grzegórska, Elżbieta Gabała, Joanna Zembrzuska, Mirosław Szybowicz, Hubert Fuks, Anna Szymczyk, Anna Zielińska-Jurek, Marek Sikorski, Teofil Jesionowski

PII: S1010-6030(22)00651-7
DOI: https://doi.org/10.1016/j.jphotochem.2022.114428
Reference: JPC 114428

To appear in: *Journal of Photochemistry & Photobiology, A: Chemistry*

Received Date: 10 July 2022
Revised Date: 25 September 2022
Accepted Date: 15 November 2022

Please cite this article as: A. Kubiak, A. Grzegórska, E. Gabała, J. Zembrzuska, M. Szybowicz, H. Fuks, A. Szymczyk, A. Zielińska-Jurek, M. Sikorski, T. Jesionowski, TiO_2-C nanocomposite synthesized via facile surfactant-assisted method as a part of less energy-consuming LED-based photocatalytic system for environmental applications, *Journal of Photochemistry & Photobiology, A: Chemistry* (2022), doi: https://doi.org/10.1016/j.jphotochem.2022.114428

TiO_2-C nanocomposite synthesized via facile surfactant-assisted method as a part of less energy-consuming LED-based photocatalytic system for environmental applications

Adam Kubiak[a,b*], Anna Grzegórska[c], Elżbieta Gabała[d], Joanna Zembrzuska[a], Mirosław Szybowicz[e], Hubert Fuks[f], Anna Szymczyk[f], Anna Zielińska-Jurek[c], , Marek Sikorski[a], Teofil Jesionowski[g]

[a]*Adam Mickiewicz University, Poznan, Faculty of Chemistry, Uniwersytetu Poznanskiego 8, PL-61614 Poznan, Poland*

[b]*Poznan University of Technology, Faculty of Chemical Technology, Institute of Chemistry and Technical Electrochemistry, Berdychowo 4, PL-60965 Poznan, Poland*

[c]*Gdansk University of Technology, Faculty of Chemistry, Department of Process Engineering and Chemical Technology, Narutowicza 11/12, PL-80233 Gdansk, Poland*

[d]*National Research Institute, Institute of Plant Protection, Węgorka 20, PL-60318 Poznan, Poland*

[e]*Poznan University of Technology, Faculty of Materials Engineering and Technical Physics, Institute of Materials Research and Quantum Engineering, Piotrowo 3, PL-60965 Poznan,*

[f]*Department of Technical Physics, Faculty of Mechanical Engineering and Mechatronics, West Pomeranian University of Technology, Al. Piastów 19, PL-70310 Szczecin, Poland*

[g]*Poznan University of Technology, Faculty of Chemical Technology, Institute of Chemical Technology and Engineering, Berdychowo 4, PL-60965 Poznan, Poland*

**Corresponding author: adam.kubiak@amu.edu.pl; Tel.: +48 61 829 17 21*

Abstract

A novel facile method was used to incorporate carbon into the titania structure. An alternative synthesis method of carbon-doped TiO_2 has been proposed by using a widely used and cheap

surfactant. During the process, cetyltrimethylammonium bromide plays a dual role, as a morphology modifier and as a carbon source. The presented approach allows obtained TiO_2-C nanostructures to be anatase nanocrystals with carbon being deposited either on the surface or between the TiO_2 nanoparticles. The innovative nature of the research subject is related to the design of cheap LED solutions and facile synthesis of TiO_2-C for use in novel energy-saving photocatalytic systems. Photocatalytic studies showed promising activity in the oxidation of 4-chlorophenol. Furthermore, it was indicated that LED-based photocatalytic systems allow a significant reduction in energy consumption compared to conventional photocatalytic sets. In addition, the high thermal efficiency of LED systems was confirmed with a thermal imaging camera. Hence, the presented novel LED photocatalytic systems can be an important part of a broad strategy for the protection of the environment.

Keywords: titanium dioxide; carbon-doped; photocatalysis; LED; energy-saving; environmental protection

1. Introduction

Currently, issues related to renewable energy technologies play a crucial role in environmental protection. An economy based on fossil fuels results in a growing amount of environmental waste, including sewage, as well as air pollutants [1–3]. This is reflected in the alarming levels of carbon dioxide in the atmosphere, which reached a concentration of 403 ppm [4]. It is well known that CO_2 resulting from oxidation of carbon in fuels during combustion accounts for the highest share of global anthropogenic greenhouse gas (GHG) emissions [5]. Nevertheless, the Paris Agreement provides a ray of hope to limit climate change by restricting the average global warming to below 2.0 °C above the preindustrial levels (1850–1900) and pursuing efforts to limit the temperature increase to 1.5 °C [6]. However, in addition to the top-down approach of

seeking to increase the share of renewable energy in total electricity production, there is also a need to continuously develop the bottom-up approach, focusing on low-energy-demand technologies.

Estimates suggest that approx. 20% of our carbon footprint is due to lighting alone. Therefore, it is one of the areas of life which requires essential development. One of the fundamental technologies that significantly reduce energy consumption in lighting is light-emitting diodes (LEDs). According to a study by IHS Markit, the use of LEDs to illuminate buildings and outdoor spaces reduced CO_2 emissions by nearly 570 million tons in 2017 [7]. What is equally important, LEDs are manufactured using 100% recyclable materials, unlike traditionally used bulbs, which means they should not end up in landfill sites at the end of their lives. Therefore, a lighting transformation involving switching to LED light sources could be observed in recent years [8]. However, the transition to LEDs did not go smoothly in all possible areas; for example, these changes did not affect advanced technological processes based on light sources, e.g., photocatalysis [9]. After analyzing the phenomenon of photocatalysis, two crucial aspects that have an impact on the obtained pollutant removal efficiencies should be mentioned: photocatalyst and light source. However, in recent years, many research teams worldwide have focused solely on synthesizing advanced multicomponent photoactive materials, putting aside the necessary development of the light source. Currently, two main light sources are used in photodegradation processes: xenon and mercury lamps. The technological photo-oxidation processes based on classic photocatalytic sets are limited for several reasons [10]. One is due to the harmful side effects of classic light sources, high voltage at the initial stage and cooling requirement [11]. However, the main issue is the usage of hazardous elements, including mercury and xenon, classified by the U.S. Environmental Protection Agency as a hazardous air pollutant (HAP) and very harmful to human health [12]. Furthermore, in 2013, 128 countries

have signed the Minamata Convention on mercury, providing its gradual phase-out in several products and processes by 2020 [13].

The photocatalyst is the second crucial aspect determining the effectiveness of the photocatalysis phenomenon. However, several conditions must be met for this material to be used on a large scale. First of all, it must be a material that is as cheap as possible, stable, and, equally important, facile to obtain. The photocatalytic materials must be active in the visible light range considering industrial use. Nowadays, many materials can absorb radiation in a wide range, including g-G_3N_4, $ZnTiO_3$, CuS/RGO, and others [14–17]. However, the costs of the synthesis process often exclude the possibility of their implementation on a large scale. Therefore, research is still needed to obtain a cheap and effective photocatalyst active in visible light. One of the potential photocatalysts may be commercially obtained TiO_2 P25 Aeroxide. However, attention should be paid to its lack of homogeneity. Ohtani et al. [18] reported a different anatase-rutile ratio, which had a crucial impact on the photocatalytic activity tested. Based on the available literature, another pathway to activation of TiO_2 in the visible light range might be possible . Piątkowska et al. [19] noted that the introduction of carbon atoms into the TiO_2 structure could lead to a narrowing of the band gap and thus to an improvement in visible light absorption. The most common approaches include the utilization of sugars and organic acids, as well as (bio)polymers as carbon sources. However, apart from the presence of an impurity in the structure of the photocatalyst, the other physicochemical parameters are also crucial. Gerbreders et al. [20] found that the designed morphology plays a crucial role in determining the properties of the final materials. Therefore, it seems promising to use surfactants for this purpose, which can play a double role in doping TiO_2 with carbon. They are morphology control agents as well as a carbon source for the doping pathway during synthesis. Such a multifunctional use of available resources is important from an industrial and environmental protection point of view.

In this research, TiO_2-C nanostructures were obtained by facile surfactant-assisted synthesis and were applied to photocatalytic degradation of 4-chlorophenol. Commercial consumer LED solutions for the photooxidation pathway were used for the first time. The high efficiency of 4-chlorophenol removal under both LEDs and sunlight has been confirmed with HPLC. The electricity consumption of mercury and xenon sets and LED systems was compared to evaluate the energy-efficiency of the processes applied in this research. The presented path focused on two crucial aspects of the field of photocatalysis, i.e., the design of novel LED solutions, as well as the fabrication of TiO_2-C nano-structure by facile surfactant-assisted process, allowing for the development of a novel approach to photocatalysis, consistent with the assumptions of green chemistry as well as sustainable development.

2. Materials and Method

2.1. Materials

Titanium(IV) isopropoxide (TTIP, 97%), cetrimonium bromide (CTAB, for synthesis), isopropanol (IPA, 99.5%) and ammonia solution ($NH_3 \cdot H_2O$, 25%) were purchased from Sigma-Aldrich (USA). All reagents were of analytical grade and used without any further purification. The water used in all experiments was deionized.

2.2. Synthesis of TiO_2-C nano-structures

In a typical synthesis, 1 dm^3 of IPA and 40 cm^3 of TTIP were introduced into an IKA Laboratory reactor equipped with an anchor stirrer (IKA Werke GmbH & Co, Germany). Then a 100 cm^3 of 2% solution of CTAB in IPA was prepared, which was also placed in the reactor after the resulting solution was stirred at a constant speed of 150 rpm for 60 min. After this time, 100 cm^3 of 25% ammonia solution was added at a constant rate (5 cm^3/min) using an ISM833A peristaltic pump (ISMATEC, Germany). The reaction mixture was stirred at room temperature at 150 rpm for 24 h. Next, the obtained colloidal suspension was left to gel. The residue was washed several times with deionized water and ethanol to remove impurities. Lastly, the powder

was dried at 100 ºC for 24 h and, after that, calcined in the temperature range of 300-400 ºC for 2 h (in increments of 25 ºC) (Nabertherm P320 Controller, Germany). In addition, a reference sample was also obtained that had not been calcined (TiO_2_0). The obtained materials were marked as TiO_2_calcination temperature, e.g., TiO_2_300, TiO_2_325, etc.

2.3. Analysis of TiO_2-C structures

The physicochemical characterization of the synthesized TiO_2-C nanocomposite included the determination of elemental analysis, characteristic of functional group (FTIR), diffuse reflectance spectroscopy (DRS), morphology (TEM), crystalline structure (XRD, Raman), electron paramagnetic resonance (EPR), the parameters of the porous structure (low-temperature N_2 sorption). The detailed data on the conducted physicochemical analyses are presented in Supplementary Materials.

2.4. Photocatalysis

The photo-oxidation properties of the TiO_2-C nanostructure were tested in the photo-oxidation of 4-chlorophenol using LEDs and sunlight as light sources. The measurement procedure is described by us elsewhere [21]. Detailed information on the photocatalytic activity tests performed is provided in the Supplementary Materials.

3. Results and Discussion

3.1. FTIR spectroscopy

First, to confirm the effectiveness of the proposed facile surfactant-assisted synthesis and determine the characteristic functional groups for the obtained nanocomposites, FTIR analysis (Fig. 1) was performed.

Figure 1

Based on the FTIR spectrum for reference titanium dioxide (TiO_2_0), in addition to the bands for titania (≡Ti-O and -OH) [22], characteristic bands corresponding to CTAB [23] were also observed, which confirms effective modification of the surface of TiO_2 using the facile

surfactant-assisted technique. Most of the CTAB bands previously observed were not found [24]. In addition to the bands characteristic for the stretching vibrations of =Ti-O (750 cm^{-1}), the hydroxyl groups (3500 cm^{-1}), and the physically bound water (1600 cm^{-1}), a band was observed that originated from the bending vibrations of the CH group (1400 cm^{-1}), which indicates the presence of carbon in the analyzed materials. However, it should be noted that this band disappears as the temperature of the heat treatment increases.

In addition, a decrease in the intensity of characteristic bands for hydroxyl groups, as well as physically bound water, was observed with the increase in the temperature of the calcination process, which can be explained by the closure of the porous structure due to crystallization of TiO_2 which is well described in the available scientific literature.

3.2. Elemental analysis

To confirm that surfactants (incl. CTAB) can be a carbon source in the titania doping process, a series of elemental analyzes were performed to determine the contents of carbon, nitrogen, hydrogen, and sulfur (Table 1).

Table 1

Among the titanium materials analyzed, the reference sample TiO_2 had the highest content of the analyzed elements. The high content of carbon, hydrogen, and nitrogen for the reference material is due to the presence of CTAB in the reaction medium, which in turn confirms that the surfactants are bound to the reference titania. For samples calcined in the temperature range of 300-400 ºC, a decrease in the content of all elements is observed, which is expected because the process is carried out in air. However, regardless of the temperature used, the lowest weight loss was recorded for carbon, whose content for the TiO_2_400 sample is 2.259%.

3.3. Diffuse reflectance spectroscopy (DRS)

Taking into account the presence of carbon in the structure of the synthesized materials, which could modify the light interaction with studied materials, diffuse reflection spectroscopy (DRS) was performed (Fig. 2).

Figure 2

Compared to reference TiO_2 P25, there were obvious changes in F(R) visible-light absorption for the prepared TiO_2-C samples. The spectral edge indicates a gradual decrease in the optical band gap of the TiO_2-C samples as the calcination temperature increases. The results showed that the TiO_2-C nanocomposite could be activated under visible light irradiation. The band gap energy (E_g) was calculated from the Kubelka-Munk theory [25].

In the case of the non-calcined sample (TiO_2_0), the band gap of 3.3 eV was determined. Similar results for the amorphous sample were also presented in the study by Prasai et al. [26]. The authors indicated that in amorphous TiO_2 most of the titanium and oxygen atoms tend to be sixfold and threefold coordinated, respectively, showing a similar local structure to the crystalline form titanium dioxide. Therefore, the electronic structures of amorphous TiO_2 are similar to the electronic structures crystalline with anatase in many respects. Therefore The Γ-point band gaps of amorphous titanium dioxide are comparable to the calculated results for bulk crystalline titania. For samples calcined at 300-400 °C, the band gap energies were 2.85 to 3.2 eV, respectively. The results suggested that the band gap of TiO_2-C samples treated at 300-375 ºC was narrower than that of reference TiO_2 and increased with increasing calcination temperature. In the case of TiO_2_400, the energy of the band gap was observed similar to the values in the literature. The observed variation of the energy band gap may depend on the carbon content and crystal structures of TiO_2. The presence of carbon in the TiO_2 nanostructure may have created interface states, which may have resulted in narrowed band gaps. On the other hand, the obtained value of the band gap energy for the TiO_2_400 material indicates the probable removal of carbon dopants from the TiO_2 structure.

On the basis of the available scientific literature, it can be indicated that changes in the band gap are produced when a C atom is introduced into the bulk structure of the anatase. Moreover, Yang et al. [27] concluded that spin-polarized impurity levels of orbital C 2p character are introduced when the C atom behaves as an anion (C@O). On the other hand, Heffner et al. [28] suggest that the replacement of an O atom (C@O) is energetically more favorable than the replacement of a Ti atom (C@Ti), therefore it is possible to creat Ti^{3+} centers. In addition, all models related to the introduction of impurity levels in the band gap analyzed by the authors resulted in an absorbance shift towards the visible regions.

Carbon in the C-TiO_2 samples may have played two crucial roles. First, an impurity (or a lattice defect of TiO_2) forms interface states that effectively reduce the band gap. Additionally, it could be a promoter for the formation of anatase crystals from the amorphous phase. This effectively reduced the band gap of the TiO_2 to approximately 2.85-2,97 eV. Therefore, it resulted in the shifting of the absorption toward the visible-light range for the TiO_2-C nanocomposites mentioned above.

3.4. Morphology and microstructure

Bearing in mind that particle size control, particularly on the nanoscale, is fundamental for materials applications, transmission electron microscopy (Fig. 3) was carried out.

Figure 3

The main advantage of the sol-gel method used in our work is the ability to control the microstructure of the synthesized material, which is confirmed by the image obtained for the reference TiO_2 sample (Fig. 3a) [29]. For this material, amorphous nanometric particles were obtained; in addition, these particles form larger aggregates about 200-250 nm in diameter. In our work, titania products were subjected to temperatures of 300-400 °C. However, even such minor differences in the calcination temperature resulted in apparent changes in the morphology of the obtained products. In the case of samples calcined at temperatures between 300-350 °C

(Fig. 3b-d), two fractions can be observed – amorphous and with a specific shape, e.g., cubic or octahedral. With TiO_2_375 (Fig. 3e) and TiO_2_400 (Fig. 3f), only particles characteristic of crystalline forms of TiO_2 were observed, e.g., rod and spherical [30].

However, to thoroughly analyze the microstructure of the TiO_2 samples obtained, additional high-resolution analysis (HR-TEM) and fast Fourier transformation (FFT) were performed. The presented HR-TEM images (Fig. 4) indicate that the TiO_2-C nano-structures are nanocrystals also with the presence of an amorphous structure. The presence of the amorphous area for the analyzed materials can be associated with two phenomena: the presence of amorphous TiO_2 particles and the admixture of carbon. The crystallization that occurs at higher temperatures is confirmed by additional spots on the FFT images. However, the presence of carbon was also confirmed by elemental analysis and EPR. Since both the TiO_2 part and the carbon dopant have an amorphous structure, it is difficult to accurately assign the indicated regions to one component. However, according to the available scientific literature, the carbon dopant is presented in the form of a carbon layer that covers the nanocrystalline TiO_2 particles and therefore can modify the absorption of photons, which is crucial when considering the use of materials in photocatalytic processes [31]. However, Li et al. [32] reported that the graphene-coated Langmuir–Blodgett film had a high transmittance in the visible wavelength range, suggesting that visible light can penetrate the carbon film and be absorbed by C-TiO_2.

Figure 4

3.5. Crystal structure

The crystallinity characteristics of the obtained TiO_2-C nanocomposites were determined using X-ray diffraction analysis (XRD) and Raman spectroscopy, as shown in Fig. 5.

Figure 5

At the outset, note that regardless of the calcination temperature used, the anatase (crystallographic database card no. 9009086) crystalline structure (space group $I4_1/amd$, no. 141) was observed [33]. Furthermore, crystalline planes such as (101), (103), (004), (200), (105), (211), (213), (116), (220), and (215) were found in the nanomaterials analyzed [34]. However, the average crystallite size was determined to characterize the difference in the crystalline structure of the oxide materials obtained. The average crystallite size was calculated using the Scherrer equation.

Based on the results of crystallinity (Table 1), it was found that the conditions of the calcination process have a crucial influence on the size of the TiO_2 crystallites. In the case of samples subjected to treatment at 300-350 ºC, the crystallite size was 11.2-11.8 nm. The further increase in the calcination temperature resulted in a step increase in the crystallite size equalling 12.8 nm for the TiO_2_375 material. This increases the average size of the crystallites by over 1 nm compared to the materials mentioned above (TiO_2_300, TiO_2_325, TiO_2_350). For the sample calcined at 400 ºC, the average crystallite size was 14.2 nm. It increases by more than 2 nm compared to materials processed in the temperature range of 300-350 ºC. When the remaining crystallinity parameters are analyzed, a decrease in both the *a* and *c* lattice parameters of the unit cell should be noted with increasing calcination temperature. Mahia et al. [35] have already described this phenomenon and have shown that the structure of oxide materials is sensitive to the preparation method, particularly the temperature of calcination.

However, Raman spectroscopy was performed to characterize the crystal structure of the obtained nanomaterials comprehensively. Figure 5 shows the Raman spectra of the samples calcined at different temperatures. The observed peaks at 140 cm^{-1} ($E_{g\text{-symmetry}}$), 195 cm^{-1} (E_g), 395 cm^{-1} (B_{1g}), 520 cm^{-1} ($B_{1g}+A_{1g}$), and 640 cm^{-1} (E_g) can be attributed to the characteristics of the anatase phase [36], which indicates that the anatase is the predominant phase structure at all calcination temperatures. However, there is a change in the peak position as calcination

temperature increases, and the intensities of the peaks are different, as shown in Supplementary Materials Fig. S2. The shift of the Raman peak wavenumber may be due to a size change, a lattice disorder, or defects such as oxygen vacancies [37]. Furthermore, the decrease in FWHM indicates that crystallinity is enhanced when calcined at higher temperatures, which is consistent with the results of the XRD analysis [38].

Currently, TiO_2-C nanocomposites can be obtained in many ways. For this purpose, various sources of carbon are used, including sugars, organic acids and (bio)polymers. Alternatively, the carbon source can be integral to the TiO_2 precursor, as exemplified by titanium(IV) isopropoxide and titanium(IV) butoxide. However, regardless of possible synthetic pathways, TiO_2-C compounds are characterized primarily by the crystal structure of anatase, confirmed in our research. Incorporation of carbon into the TiO_2 structure can be demonstrated by changes in the lattice parameters (determined from the XRD spectra) and changes in the position of the bands on the Raman spectrum, which was observed for synthesized nanocomposites.

3.6. EPR spectra of TiO_2-C nanocomposites

The presence of localized paramagnetic centers as a result of the formation of defects and oxygen and titanium vacancies in the crystal structure of TiO_2-C nanoparticles that are responsible for their photocatalytic properties was examined by EPR spectroscopy. It is known that no defected TiO_2 contains Ti^{4+} in its structure and due to the absence of unpaired electrons in its electronic configuration in the EPR spectra no signal should be observed. In the calicnated C doped antanase TiO_2 nanostuctures the unpaired electrons or paramagnetic centres such as the oxygen vacancy (one electron trapped) in the TiO_2 crystals and as Ti^{3+} may be present, usually at temperatures below 120 K [39,40].

For the anatase TiO_2 and the synthesised TiO_2-C nanocomposites, the EPR spectra were measured in the temperature range of 80-300 K, but no changes were observed in the position and width of the line. Figure 6 a compares the EPR spectra of the TiO_2 and TiO_2-C nanostructures obtained at room temperature (RT), while Figs. 6 b, c present the spectra recorded for the chosen samples at RT and ca 82 K. As expected, the EPR spectra of the reference sample TiO_2_0 were completely silent, which indicates the high quality of this sample. However, in EPR spectra the paramagnetic centers that can be generated from electron trapping sites through the oxygen radicals in oxygen vacancies or electrons ($Ti^{4+}O_2^{\bullet-}$, $Ti^{4+}O^{\bullet-}$ or Ti^{4+}/hole/e−) can be visible for TiO_2 synthesized by using different methods [41,42]. The signals ofTi^{3+} ions can be detected due to the of the partial reduction of Ti^{4+} ($e^- + Ti^{4+} = Ti^{3+}$) [39]. For the TiO_2-C nanostructures synthesised here, the EPR signal consists of two parts of resonance spectra: a wider line (c.a. 0.39 mT line width) located at spectroscopic value g = 2.0041 with, and a very narrow line (0.06 mT line width) located at g = 2.0014. Additionally, the narrow signal shows asymmetry in samples TiO_2_350 and TiO_2_375 resulting in visible splitting of the line. These narrow signals can be assigned to the formation of the $Ti^{4+}O_2{-}Ti^{4+}O^{\bullet-}$ arrangement on anatase [43]. This signal is the most intense in the sample heated at 375 °C. Additionally, for samples TiO_2_350 and TiO_2_375, the signal with low intensity at g = 2.0024 was found. These results indicate the presence of at list two defects in the crystal structure of carbon doped TiO_2 nanostructures synthesized at 325, 350 and 375 °C. Several narrow lines instead of one result from a disturbance in the local network environment around the oxygen vacancy ($O^{\bullet}$) in anatase.

Similar EPR signals have been observed after doping of TiO_2 in [44–47]. Furthermore, the intensity of the signal was also observed to increase significantly increase with the increasing amount of the doped carbon in anatase [39]. This evidence that the presence of carbon favours creation of oxygen vacancies. In the work presented by Minnekhanov et al. [45] a single line

was found at g = 2.003 for the surface C doped TiO_2, but for volume carbon doped TiO_2 signals at the values of the g- factor g_1=2.043, g_2=2.0027, g_3=2.0013were found.

The intrinsic band gap of anatase was shown to be significantly modified by forming mid-gap states or by its narrowing due to the presence of radicals O• and, consequently, to the reduction of energy of band gap energy [44]. The energy reduction is related to the EPR signal increase. Yang et al. [48] have demonstrated that the heating rate or the temperature of calcination can significantly influence on the generation of oxygen vacancies as TiO_2 is doped with carbon. Herein, for synthesized carbon doped TiO_2 the largest signal splitting was observed for the sample TiO_2_375 in comparison to sample TiO_2_400 which is doped approximately by the same amount of carbon (Table 1). Probably increasing the calcination temperature above 375 ^oC, does not favor to the creation of oxygen vacancies.

The analysis of the EPR spectra for the TiO_2_300 and TiO_2_400 samples showed the presence signal at g = 2.0042, which is attributed to the electrons trapped in the oxygen vacances in the crystal structure of TiO_2 [45]. A similar signal at g =2.005 was confirmed in the carbon doped TiO_2 in work presented by Reyes-Gracia et al. [44]. The signal for carbon doped TiO_2_400 (Fig. 6a) nanostructures is less intensive than for the TiO_2_300 sample. The change in integral intensity of this signal is reduced compared to the sample TiO_2_300. This can be a result of the lower concentration (by about 55%) of C atoms in sample TiO_2_400 (see Table 1) in relation to the TiO_2_300 sample. It was found that the band gap for this sample increased by approximately 0.35 eV in relation to the TiO_2_300 sample, in which more carbon radicals (C•) can contribute with CO^- radicals to the broad signal observed in the EPR spectra [48]. Additionally, the samples with higher carbon content in the crystal structure of anatase TiO_2 can have higher content of paramagnetic centers [45]. Di Valentin et al. [49] showed that in carbon doped TiO_2 localized states are formed but their charter and concentration dependent both on the oxygen temperature/pressure conditions during synthesis and the content of doping

carbon atoms. In addition, in carbon containing TiO_2, the signal corresponding to Ti^{+3} centers is usually present at g = 1.98 and is detected in EPR spectra at temperatures below 120 K [46]. Analysis of the EPR spectra in the range from room temperature (RT) to 80 K does not confirm the presence of Ti^{+3} centers in the crystal structure of the synthesized carbon doped TiO_2 nanostructures. The representative spectra for the sample TiO_2_300 and TiO_2_375 at RT and at ca 80 K are presented in Fig. 6 b-c. The position of the signals with temperature did not change and characteristic signal of the trapped electrons at Ti^{3+} sites in anatase, which is generally observed at g < 2.0 [48] was absent. These results confirm that carbon doping in the synthesized TiO_2 favors the formation of oxygen vacancies that are responsible for their photocatalytic performance.

Figure 6

3.7. Porous structure

The essential element of the comprehensive characterization of each new material is the determination of the parameters of the porous structure. The obtained N_2 adsorption-desorption isotherms are presented in Fig. 7, while the porous structure parameters are shown in Table 1.

Figure 7

The nitrogen sorption isotherms presented, all synthesized nanocomposites are characterized by the IV-type isotherm with the H1 hysteresis loop [50], which confirmed the mesoporous nature of the materials analyzed. The H1 loop indicates that the nanocomposites consist of agglomerates or compacts of approximately uniform shape in a fairly regular array, and hence to have narrow distributions of pore size [50]. Moreover, it should be noted that synthesized nanostructure materials have a similar range of hysteresis loops equal to p/p_0 – 0.33-0.99 regardless of the calcination temperature.

Based on the textual structure data for the reference sample (TiO_2_0), the BET surface area of 382 m^2/g was recorded. Furthermore, total volume and pore diameter were 0.329 cm^3/g and 35

nm, respectively. The results obtained are similar to the BET surface area obtained by other research teams for amorphous materials based on TiO_2. For example, in our earlier work, we obtained amorphous titanium dioxide with a specific surface area of approximately 450 m^2/g [51]. On the other hand, Shao et al. [52] produced amorphous TiO_2 by the sol-gel method with a BET surface area of 273 m^2/g. The calcination process at the temperature of 300 ºC resulted in an almost twofold reduction in the specific surface area (TiO_2_300=173 m^2/g), while a further increase in temperature to 400 ºC led to a nearly ninefold decrease in surface area (TiO_2_400=45 m^2/g). The observed decrease in the BET surface area is due to two main processes: crystalline growth and closure of the porous structure due to sintering.

On the basis of low-temperature nitrogen sorption results, it was shown that the temperature of the calcination process had a significant impact on the parameters of the porous structure, in particular the value of the BET surface area and the average pore diameter. However, it should be noted that the facile surfactant-assisted synthesis proposed by us allowed not only the incorporation of carbon into the TiO_2 structure, but it also resulted in a mesoporous character, as indicated by the wide hysteresis loop type H3. The mesoporous nature is a crucial issue to obtain promising photocatalysts.

3.8. Photocatalysis test

The crucial point of the research was to determine the photocatalytic activity of the obtained TiO_2-C nanocomposite in the degradation of the phenol derivative 4-chlorophenol (4-CP). Photooxidation tests were performed using the novel LED solution based on commercial visible LEDs. The photo-oxidation curves are presented in Fig. 8. Additionally, the degree of photodegradation of 4-chlorophenol was determined using HPLC. The data collected are summarized in Table S1 in the Supplementary Materials.

4-Chlorophenol was selected as a model pollutant due to its toxicity at a concentration of only a few μg/l [53,54]. Abnet et al. [55] have shown that chlorophenols and phenoxyacetic acid

herbicides have induced cancer in rodents. For this reason, the World Health Organization established a permissible concentration of 4-CP at the level of 2 μg/dm^3 in drinking water [56]. On the other hand, typical 4-CP concentrations in wastewater are 300-400 μg/l [57,58]. Keeping this in mind, it is essential to continuously monitor chlorophenol concentration in the aquatic environment and further develop methods for its removal.

Figure 8

In the presented research, three LED light sources with different color temperatures were used. It is well known that the color temperature affects the spectrum of the light source and, therefore, the effectiveness of photoactive processes. For this reason, LED solutions with various parameters were selected for the research. The color temperature of 3500K corresponds to warm white. The 4500K color is marked as natural light, direct sunlight, but without UV. On the other hand, 6500K can be assigned to a cool white sky and a cloudy sky. It should be noted that the color temperature of the LED solutions had a high impact on the removal efficiency of 4-chlorophenol. However, the material calcined at 350 ºC had the highest 4-CP removal efficiency regardless of the LEDs used. Based on the photo-oxidation tests conducted for TiO_2_350, it was shown that the use of a warm white-light source removed approximately 92% of 4-CP after 6 h. Using a 4500K LED solution gave nearly 96% of photodegradation efficiency at 6h. On the other hand, using a cool white light source obtains a similar 4-CP removal efficiency (95%) after 3 h of irradiation. The lowest removal efficiency of the investigated phenol derivative was obtained for the TiO_2_300 material. The photodegradation efficiency was 60%, 72%, and 95% after 6 h of irradiation for the 3500K, 4500K, and 6500K LED light sources. On the contrary, the remaining materials (TiO_2_325, TiO_2_375, and TiO_2_400) had a 4-CP removal efficiency of 75-80% for warm white light (3500K) and 80-90% for neutral white light (4500K). Using a light source with a color temperature of 6500K caused almost complete degradation of 4-CP (95-99%) for the samples mentioned above. Furthermore, the obtained

photocatalysts were tested under sunlight. In the case of using natural light for all the nanocomposites tested, the satisfactory results of removing the tested contamination (over 90%) after the exposure time of 6 hours were confirmed. As also seen with LED solutions and sunlight, the highest 4-CP removal efficiency was demonstrated by TiO_2_350 material – over 99% after 6 h and almost 90% after 3 h of irradiation. On the other hand, the lowest photoactivity was found in the material TiO_2_300, which achieved 90% of the photodegradation efficiency after 6 h of exposure to sunlight. Based on the obtained results of photooxidation tests, the synthesized materials can be arranged according to the decreasing efficiency of 4-chlorophenol degradation: TiO_2_350> TiO_2_325> TiO_2_375> TiO_2_400> TiO_2_300. Additionally, for each of the analyzed light sources, an experiment was also conducted without the addition of a photocatalyst (photolysis). For LED light sources it was <5%, and for sunlight it was about 10%. The increase in photolysis efficiency for the solar experiment is due to the use of UV light, which is part of the sunlight spectrum. In addition, photo-oxidation experiments were also carried out using commercial titanium dioxide P25. Regardless of the light source used, the degradation efficiency of P25 was similar to that of the TiO_2_300 sample. The lower efficiency of the commercial material compared to the synthesized TiO_2-C samples results mainly from the difference in the mechanism of the photo-oxidation process. For P25, there is a type II heterojunction between anatase and rutile, while for TiO_2-C samples, surface defects caused by carbon incorporation into the TiO_2 structure are responsible for visible light activity.

The TiO_2-C nano-systems with the highest removal efficiency (TiO_2_350 sample) were selected for reusability studies. Five successive cycles were carried out to evaluate the effectiveness of the photocatalysts after their recovery. The data are shown in Supplementary Materials Fig. S3. The TiO_2_350 samples were separated from the aqueous solution by filtration at the end of the first photo-oxidation tests. The separated nanocomposite was then reused without any

purification. In each case, the efficiency of 4-chlorophenol removal using TiO_2_350 nano-systems was above 90%, even after 5 catalytic cycles, regardless of the vis-LED light sources used. Such a result confirms that the synthesized systems can be used many times in photo-oxidation processes.

The presented research focused on two crucial issues in the field of photocatalysis, i.e., a light source and a photocatalyst. During the study, the effect of the photocatalyst calcination temperature and the change in the color temperature of the light source on the efficiency of the removal of 4-chlorophenol was investigated. According to the available literature [59], the temperature of calcination determines a number of physicochemical parameters, including crystal and textural structure, morphology, etc. However, these parameters are closely related to the subsequent use in photo-oxidation processes. For materials with the highest photoactivity (TiO_2_325 and TiO_2_350), a similar crystallite size (11.3-11.8 nm) and surface area (92-100 m^2/g) were observed. Improvement in crystallinity for the TiO_2_375 and TiO_2_400 samples led to a significant decrease in the BET surface area in the samples, which consequently resulted in lower 4-chlorophenol removal efficiency. For the TiO_2_300 sample, the crystallite size (11.1 nm) was similar to that of the samples with the TiO_2_325 and TiO_2_350 materials. However, the high value of the BET surface area and low intensity of the Raman spectrum bands may indicate an amorphous TiO_2 phase. On this basis, it was confirmed that the high photoactivity for TiO_2_325 and TiO_2_350 materials should be explained by the favorable interaction between the specific crystal structure and the surface area. Furthermore, results indicate that one of the factors in improving the photoactivity of these materials is the presence of nanocrystal structures with carbon deposited on the TiO_2 surface. The influence of carbon on TiO_2 photoactivity was confirmed, among other things, by Lin et al. [60]. The authors noted that the carbon significantly affects both band gap narrowing and the electronic structure of the synthesized material, thus improving its photoactivity under visible-light irradiation. They are

focusing on the effect of the color temperature of LED on the efficiency of pollutant removal. It should be noted that the second issue presented in the paper, to the best of our knowledge, has not been described in the scientific literature so far. Photocatalysis using LED applications is gaining popularity. This is mainly due to the life expectancy of LEDs, which is almost 20 times longer than a traditional incandescent light source. Also, LEDs are manufactured using 100% recyclable materials, unlike traditional bulbs, which means they should not end up in landfills at the end of their lives. However, most scientific works focus on ultraviolet (UV) light, neglecting the possibility of using commercial vis-LED solutions. One of the few vis-LED solutions was presented by Li et al. [61]. The authors used LEDs with a wavelength of 470 nm for the air purification process. Zhang et al. [62] improved the disinfection performance of human adenoviruses using a vis-LED photocatalytic membrane reactor. However, when commercial vis-LED diodes are used, it is necessary to study the basic parameter that determines the spectrum of light because the color temperature has a determining influence, in particular, on the range of blue light. Changing the color of the light from 3500-6500K results in a more than fivefold increase in the intensity of blue light. The presence of carbon and reduction of the band gap energy in the synthesized materials are taken into account. This may explain the observed increase in 4-chlorophenol removal efficiency for the 6500K LED solution. However, attention should be paid to the difference in the photodegradation efficiencies between the 4500 K LED light source and sunlight. Despite that, 4500K LEDs are described as close to natural light, similar to sunlight. They do not contain the UV range present in natural sunlight at about 5%. Therefore, it was possible to obtain higher 4-CP removal results for sunlight than the 4500K LED solution. The most advantageous light source for photocatalytic processes is sunlight from the point of view of availability. However, its implementation in wastewater treatment systems seems limited due to high costs and large

footprint demand for installation. Additionally, the efficiency of the reactor depends on the direction, intensity, and availability of solar light [63,64].

One of the critical aspects of photooxidation processes is the degradation mechanism of the tested pollutant. The photoactivity of the synthesized TiO_2-C nanocomposites under irradiation with commercial consumer LEDs can be explained by the appearance of a new impurity energy level above the VB caused by the C-doping of TiO_2. The band gap is narrowing, and the TiO_2-C nanocomposite can absorb visible light. The proposed mechanism of 4-chlorophenol photooxidation is shown in Fig. 9.

Figure 9

The mechanism of photo-oxidation, which proceeds by the generation of reactive oxygen species, e.g., $^{*}O_2^{-}$ that attack of the reactive oxygen species on the para position of the aromatic ring and subsequent loss of chlorine, causing the formation of phenol and hydroquinone. In further photo-oxidation, hydroquinone is converted to p-benzoquinone, which could be decomposed to the observed oxalic acid and acetic acid. During photooxidation of 4-chlorophenol, the concentration of intermediates formed (phenol, oxalic acid, and acetic acid) decreases, which can be associated with the degradation of recalcitrant chemicals to simple organic compounds. Based on the data obtained, the $^{*}OH$ radicals are the main oxidizing species responsible for the subsequent degradation of 4-chlorophenol, as described by which is in line with the available literature [65,66]. The main reactions in the photo-oxidation of 4-chlorophenol removal are hydroxylation, dihydroxylation, hydrations, and decarboxylation.

Taking into account the surface defects in the synthesized TiO_2-C systems (mainly Ti^{3+} centers), it should be noted that they can play the role of the active sites in photocatalysis, due to the formation of interfacial defect structure and band tail states on the edges of CB and VB [67]. According to the work by Zhang et al. [68] under visible light irradiation, the Ti^{3+} centers were excited and electron-hole pairs were generated. The electrons generated in the conductivity

band can transfer to the Fermi level, and the holes in the valence band can migrate from the interface layer to the surface of TiO_2 and participate in photocatalytic reactions. The Authors indicate on effective to enhance the photocatalytic activity by increasing its interfacial coordinatively unsaturated defect sites (Ti^{3+} centers). Furthermore, Xu et al. [69] indicated that the existence of Ti^{3+} defects led to strengthening the absorption of light in the UV and visible light regions and further enhancing the position of the valence band, leading to overall improved photocatalytic activity toward the degradation of phenol and derivatives under visible light irradiation. The increased absorption of the described authors in the UV region explains the high activity of synthesized materials under sunlight.

It should also be noted that the photo-oxidation of 4-chlorophenol carried out under vis-LED light allowed for a high degradation efficiency compared to other materials described in the scientific literature (Table 2).

Table 2

According to the presented review of the available scientific literature on the photodegradation of 4-chlorophenol, various photocatalysts are used under visible light. The results of photodegradation efficiency obtained by us are very promising as they allow for a high degree of photodegradation of 4-chlorophenol using commercial consumer LEDs. The innovative LED light sources for photooxidation processes presented by us are important. First, they are an extraordinarily long-lifetime and energy-saving light source. Furthermore, in contrast to the solutions offered in the literature, e.g., by Villaluz et al. [70], they do not focus solely on blue light. Limiting exposure to blue light is important due to health hazards caused by circadian disruption in modern societies [74]. Obviously, the photocatalysts we synthesize absorb blue light, which is indicated by the energy of the band gap and the results of photo-oxidation tests. However, even with a 3500K light source containing a small fraction of blue light, it is possible to achieve high 4-chlorophenol removal efficiencies. Finally, commercial consumer LEDs are

primarily widespread technology, making them cheaper than other use solutions (e.g., Xe lamps, metal halide lamps, etc.). An additional advantage of the proposed solutions is a simple cooling system based on an active heat sink (equipped with a fan) instead of the solutions mentioned above where a liquid coolant is necessary.

To better understand the advantages of using consumer LEDs, a cost calculation was performed focusing solely on electricity demand. During the photodegradation process using the LED solution and for the contrast of mercury and xenon lamps, the electricity consumption was measured, shown in Supplementary Materials Table S2.

The data collected indicated that LED light sources have almost six times and 12 times less energy consumption than mercury and xenon lamps, respectively. When analyzing the phenomena of photocatalysis in visible light, attention should also be paid to the cost of the light source itself. The consumer LED solutions used in the presented research are widely available, making their prices low. On the other hand, systems based on a mercury or xenon lamp, due to high costs, can only be used on a laboratory scale. Therefore, we believe that the use of inexpensive, common consumer LEDs described by us could be a milestone in the development of photocatalysis in visible light.

However, according to the available literature [75,76], the main problem with LED technology is the possibility of overheating of the LED chip. Hence, the thermal efficiency of the systems has been investigated. Fig. 10 shows images from a thermal imaging camera for 4500 K LEDs

Figure 10

Five minutes after switching on the LED light source the average temperature of the LEDs chip was about 60 °C, while the temperature of the model pollutant solution was close to the ambient temperature and it was 26 °C. According to Fig. 10b, after the 6 h of irradiation, the temperature of the LEDs was close to the initial temperature and was 64 °C. In addition, it should also be noted that despite the high temperature of the LED chip, the degraded solution did not overheat,

after the photodegradation process its temperature slightly increased to 29 °C. According to the technical data, modern chip-on-board LEDs can reach the operating temperature in the range of 40-80 °C. Exceeding these values may result in a slow burn out of the LEDs and shortening their lifetime. Hence, it should be emphasized that the solution we propose, based on an active cooling system (with a fan), ensures high thermal efficiency of the LEDs, and thus the assumed lifetime. Additionally, It should be noted here that, to the best of our knowledge, such a characteristic of the thermal efficiency of the designed LED solutions has not been presented so far.

4. Conclusion

One of the primary purposes of the work was to propose surfactant-assisted synthesis to facilitate the incorporation of carbon into the titania structure. The presence of carbon in TiO_2 was confirmed by elemental analysis and FTIR analysis. Carbon in the TiO_2-C samples played a crucial role in forming interface states that effectively lower the band gap. It was found that the TiO_2-C nanostructures are anatase nanocrystals with carbon being deposited either on the surface or between the TiO_2 nanoparticles.

The fundamental aspect of the research was the use of a commercial energy-saving LED light source in the removal of 4-chlorophenol. During the investigation, the influence of the color temperature of the LEDs on the photooxidation efficiency was determined. The photocatalyst TiO_2 calcined at 350 °C showed the highest photocatalytic activity regarding 4-chlorophenol oxidation. The color temperature was indicated as the critical parameter determining the effectiveness of photo-oxidation. The results for the 6500K lamp were comparable to those for the 4500K lamp but at half the irradiation time. It was indicated that LED light sources have almost six times and 12 times less energy consumption than mercury and xenon lamps, respectively. Finally, the high thermal efficiency of the LED systems has been confirmed, which ensures their assumed lifetime. This confirms that the presented novel LED-based

photocatalytic systems can be a eco-friendly and cheap alternative to current setups in photocatalytic processes under visible light.

Acknowledgments: *This research was funded by the Ministry of Science and Higher Education Poland as a subsidy to Poznan University of Technology and Adam Mickiewicz University, Poznan.*

References

[1] J. Rockström, W. Steffen, K. Noone, Å. Persson, F. S. Chapin, E. F. Lambin, T. M. Lenton, M. Scheffer, C. Folke, H. J. Schellnhuber, B. Nykvist, C. A. de Wit, T. Hughes, S. van der Leeuw, H. Rodhe, S. Sörlin, P. K. Snyder, R. Costanza, U. Svedin, M. Falkenmark, L. Karlberg, R. W. Corell, V. J. Fabry, J. Hansen, B. Walker, D. Liverman, K. Richardson, P. Crutzen, J. A. Foley, A safe operation space for humanity, Nature. 461 (2009) 472–475. doi: 10.1038/461472a

[2] D. Gust, T.A. Moore, A.L. Moore, Solar fuels via artificial photosynthesis, Acc. Chem. Res. 42 (2009) 1890–1898. doi:10.1021/ar900209b.

[3] J.G. Canadell, C. Le Quéré, M.R. Raupach, C.B. Field, E.T. Buitenhuis, P. Ciais, T.J. Conway, N.P. Gillett, R.A. Houghton, G. Marland, Contributions to accelerating atmospheric CO_2 growth from economic activity, carbon intensity, and efficiency of natural sinks, Proc. Natl. Acad. Sci. 104 (2007) 18866–18870. doi:10.1073/pnas.0702737104.

[4] S. Czernik, Catalytic Catalytic Pyrolysis of Biomass. In: J. Lee, (eds) Advanced Biofuels and Bioproducts. Springer, New York (2012) 119–127. doi: 10.1007/978-1-4614-3348-4_9

[5] T.M.L. Wigley, P.D. Jones, P.M. Kelly, Global warming?, Nature. 291 (1981) 285.

doi:10.1038/291285a0.

[6] United Nations, Framework Convention on Climate Change, Adoption of the Paris Agreement. UN Doc. FCCC/CP/2015/L.9/Rev.1

[7] Y. Ku, L.M. Yan, G.K.T. Luong, Reduction of dissolved carbon dioxide in aqueous solution by UV-LED/TiO_2 process under periodic illumination, J. CO_2 Util. 41 (2020) 101283. doi:10.1016/j.jcou.2020.101283.

[8] S. Guo, Z. Yang, H. Zhang, W. Yang, J. Li, K. Zhou, Enhanced photocatalytic degradation of organic contaminants over $CaFe_2O_4$ under visible LED light irradiation mediated by peroxymonosulfate, J. Mater. Sci. Technol. 62 (2021) 34–43. doi:10.1016/j.jmst.2020.05.057.

[9] J. Chen, S. Loeb, J.H. Kim, LED revolution: Fundamentals and prospects for UV disinfection applications, Environ. Sci. Water Res. Technol. 3 (2017) 188–202. doi:10.1039/c6ew00241b.

[10] X. Li, Z. Li, Z. Xing, Z. Song, B. Ye, Z. Wang, Q. Wu, UV-LED/P25-based photocatalysis for effective degradation of isothiazolone biocide, Front. Environ. Sci. Eng. 15 (2021). doi:10.1007/s11783-020-1379-x.

[11] T.S. Natarajan, K. Natarajan, H.C. Bajaj, R.J. Tayade, Energy efficient UV-LED source and TiO_2 nanotube array-based reactor for photocatalytic application, Ind. Eng. Chem. Res. 50 (2011) 7753–7762. doi:10.1021/ie200493k.

[12] T. Deblonde, C. Cossu-Leguille, P. Hartemann, Emerging pollutants in wastewater: A review of the literature, Int. J. Hyg. Environ. Health. 214 (2011) 442–448. doi:10.1016/j.ijheh.2011.08.002.

[13] M.A. Coulter, Minamata Convention on Mercury, Int. Leg. Mater. 55 (2016) 582–616. doi:10.5305/intelegamate.55.3.0582.

[14] Y. Deng, L. Tang, G. Zeng, J. Wang, Y. Zhou, J. Wang, J. Tang, L. Wang, C. Feng,

Facile fabrication of mediator-free Z-scheme photocatalyst of phosphorous-doped ultrathin graphitic carbon nitride nanosheets and bismuth vanadate composites with enhanced tetracycline degradation under visible light, J. Colloid Interface Sci. 509 (2018) 219–234. doi:10.1016/j.jcis.2017.09.016.

[15] R. Liu, H. Ye, X. Xiong, H. Liu, Fabrication of TiO_2/ZnO composite nanofibers by electrospinning and their photocatalytic property, Mater. Chem. Phys. 121 (2010) 432–439. doi:10.1016/j.matchemphys.2010.02.002.

[16] S. Adhikari, D. Sarkar, G. Madras, Hierarchical Design of CuS Architectures for Visible Light Photocatalysis of 4-Chlorophenol, ACS Omega. 2 (2017) 4009–4021. doi:10.1021/acsomega.7b00669.

[17] C.H. Nguyen, M.L. Tran, T.T. Van Tran, R.S. Juang, Enhanced removal of various dyes from aqueous solutions by UV and simulated solar photocatalysis over TiO_2/ZnO/rGO composites, Sep. Purif. Technol. 232 (2020). doi:10.1016/j.seppur.2019.115962.

[18] B. Ohtani, O.O. Prieto-Mahaney, D. Li, R. Abe, What is Degussa (Evonic) P25? Crystalline composition analysis, reconstruction from isolated pure particles and photocatalytic activity test, J. Photochem. Photobiol. A Chem. 216 (2010) 179–182. doi:10.1016/j.jphotochem.2010.07.024.

[19] A. Piątkowska, M. Janus, K. Szymaski, S. Mozia, C-,N- and S-Doped TiO_2 Photocatalysts: A Review, Catalyss 11 (2021) 144. doi: 10.3390/catal11010144.

[20] S. Baruah, J. Dutta, Hydrothermal growth of ZnO nanostructures, Sci. Technol. Adv. Mater. 10 (2009) 013001. doi:10.1088/1468-6996/10/1/013001.

[21] A. Kubiak, A. Grzegórska, J. Zembrzuska, A. Zielińska-Jurek, K. Siwińska-Ciesielczyk, M. Janczarek, P. Krawczyk, T. Jesionowski, Design and microwave-assisted synthesis of TiO_2-lanthanides systems and evaluation of photocatalytic activity under UV-LED light irradiation, Catalysts. 12 (2022) 8. doi:10.3390/catal12010008.

[22] A. Kubiak, Z. Bielan, A. Bartkowiak, E. Gabała, A. Piasecki, M. Zalas, A. Zielińska-Jurek, M. Janczarek, K. Siwińska-Ciesielczyk, T. Jesionowski, Synthesis of titanium dioxide via surfactantassisted microwave method for photocatalytic and dye-sensitized solar cells applications, Catalysts. 10 (2020) 586. doi:10.3390/catal10050586.

[23] R.A. Campbell, S.R.W. Parker, J.P.R. Day, C.D. Bain, External reflection FTIR spectroscopy of the cationic surfactant hexadecyltrimethylammonium bromide (CTAB) on an overflowing cylinder, Langmuir. 20 (2004) 8740–8753. doi:10.1021/la048680x.

[24] G. Su, C. Yang, J.J. Zhu, Fabrication of gold nanorods with tunable longitudinal surface plasmon resonance peaks by reductive dopamine, Langmuir. 31 (2015) 817–823. doi:10.1021/la504041f.

[25] L. Diamandescu, F. Vasiliu, D. Tarabasanu-Mihaila, M. Feder, A.M. Vlaicu, C.M. Teodorescu, D. Macovei, I. Enculescu, V. Parvulescu, E. Vasile, Structural and photocatalytic properties of iron- and europium-doped TiO_2 nanoparticles obtained under hydrothermal conditions, Mater. Chem. Phys. 112 (2008) 146–153. doi:10.1016/j.matchemphys.2008.05.023.

[26] B. Prasai, B. Cai, M.K. Underwood, J.P. Lewis, D.A. Drabold, Properties of amorphous and crystalline titanium dioxide from first principles, J. Mater. Sci. 47 (2012) 7515–7521. doi:10.1007/s10853-012-6439-6.

[27] Y. Kesong, D. Ying, H. Baibiao, W. Myung-Hwan, Density functional characterization of the visible-light absorption in substitutional C-anion- and C-cation-doped TiO_2, J. Phys. Chem. C. 113 (2009) 2624–2629. doi:10.1021/jp808483a.

[28] H. Heffner, R. Faccio, I. López–Corral, C–doped TiO_2(B): A density functional theory characterization, Appl. Surf. Sci. 551 (2021) 149479. doi:10.1016/j.apsusc.2021.149479.

[29] T. Guo, M.S. Yao, Y.H. Lin, C.W. Nan, A comprehensive review on synthesis methods

for transition-metal oxide nanostructures, CrystEngComm. 17 (2015) 3551–3585. doi:10.1039/c5ce00034c.

[30] X. Chen, S.S. Mao, Titanium dioxide nanomaterials: Synthesis, properties, modifications and applications, Chem. Rev. 107 (2007) 2891–2959. doi:10.1021/cr0500535.

[31] S.H. Wang, T.K. Chen, K.K. Rao, M.S. Wong, Nanocolumnar titania thin films uniquely incorporated with carbon for visible light photocatalysis, Appl. Catal. B Environ. 76 (2007) 328–334. doi:10.1016/j.apcatb.2007.06.001.

[32] X. Li, G. Zhang, X. Bai, X. Sun, X. Wang, E. Wang, H. Dai, Highly conducting graphene sheets and Langmuir-Blodgett films, Nat. Nanotechnol. 3 (2008) 538–542. doi:10.1038/nnano.2008.210.

[33] A.J. Haider, Z.N. Jameel, I.H.M. Al-Hussaini, Review on: titanium dioxide applications, Energy Procedia. 157 (2019) 17–29. doi:10.1016/j.egypro.2018.11.159.

[34] M.T. Noman, M.A. Ashraf, A. Ali, Synthesis and applications of nano-TiO_2 : a review, Environ. Sci. Pollut. Res. 26 (2019) 3262–3291. doi:10.1007/s11356-018-3884-z.

[35] J. Mahía, A. Vieiro, J. Mira, J. Rivas, M.A. López-Quintela, S.B. Oseroff, Influence of calcination temperature on lattice parameters and particle size of R_2CuO_4 compounds (R=Gd, Nd) prepared by a sol-gel method, J. Solid State Chem. 122 (1996) 25–30. doi:10.1006/jssc.1996.0076.

[36] Z. Wu, F. Dong, W. Zhao, H. Wang, Y. Liu, B. Guan, The fabrication and characterization of novel carbon doped TiO_2 nanotubes, nanowires and nanorods with high visible light photocatalytic activity, Nanotechnology. 20 (2009). doi:10.1088/0957-4484/20/23/235701.

[37] X. Yu, B. Kim, Y.K. Kim, Highly enhanced photoactivity of anatase TiO_2 nanocrystals by controlled hydrogenation-induced surface defects, ACS Catal. 3 (2013) 2479–2486. doi:10.1021/cs4005776.

[38] F. Dong, S. Guo, H. Wang, X. Li, Z. Wu, Enhancement of the visible light photocatalytic activity of C-doped TiO_2 nanomaterials prepared by a green synthetic approach, J. Phys. Chem. C. 115 (2011) 13285–13292. doi:10.1021/jp111916q.

[39] M. Chiesa, M.C. Paganini, S. Livraghi, E. Giamello, Charge trapping in TiO_2 polymorphs as seen by Electron Paramagnetic Resonance spectroscopy, Phys. Chem. Chem. Phys. 15 (2013) 9435–9447. doi:10.1039/c3cp50658d.

[40] Q. Yi, Y. Zhou, M. Xing, J. Zhang, Vacuum activation-induced Ti^{3+} and carbon co-doped TiO_2 with enhanced solar light photo-catalytic activity, Res. Chem. Intermed. 42 (2016) 4181–4189. doi:10.1007/s11164-015-2268-y.

[41] Z. Wang, W. Ma, C. Chen, H. Ji, J. Zhao, Probing paramagnetic species in titania-based heterogeneous photocatalysis by electron spin resonance (ESR) spectroscopy-A mini review, Chem. Eng. J. 170 (2011) 353–362. doi:10.1016/j.cej.2010.12.002.

[42] X. Pan, M.Q. Yang, X. Fu, N. Zhang, Y.J. Xu, Defective TiO_2 with oxygen vacancies: Synthesis, properties and photocatalytic applications, Nanoscale. 5 (2013) 3601–3614. doi:10.1039/c3nr00476g.

[43] P. Rychtowski, B. Tryba, H. Fuks, M.Á. Lillo-Ródenas, M.C. Román-Martínez, Impact of TiO_2 surface defects on the mechanism of acetaldehyde decomposition under irradiation of a fluorescent lamp, Catalysts. 11 (2021) 1281. doi:10.3390/catal11111281.

[44] E.A. Reyes-Garcia, Y. Sun, K.R. Reyes-Gil, D. Raftery, Solid-state NMR and EPR analysis of carbon-doped titanium dioxide photocatalysts (TiO_2-$_x$$C_x$), Solid State Nucl. Magn. Reson. 35 (2009) 74–81. doi:10.1016/j.ssnmr.2009.02.004.

[45] A.A. Minnekhanov, D.M. Deygen, E.A. Konstantinova, A.S. Vorontsov, P.K. Kashkarov, Paramagnetic properties of carbon-doped titanium dioxide, Nanoscale Res. Lett. 7 (2012) 2–5. doi:10.1186/1556-276X-7-333.

[46] E.A. Konstantinova, A.I. Kokorin, S. Sakthivel, H. Kisch, K. Lips, Carbon-doped

titanium dioxide: Visible light photocatalysis and EPR investigation, Chimia 61 (2007) 810–814. doi:10.2533/chimia.2007.810.

[47] G. Liu, C. Han, M. Pelaez, D. Zhu, S. Liao, V. Likodimos, N. Ioannidis, A.G. Kontos, P. Falaras, P.S.M. Dunlop, J.A. Byrne, D.D. Dionysiou, Synthesis, characterization and photocatalytic evaluation of visible light activated C-doped TiO 2 nanoparticles, Nanotechnology. 23 (2012). doi:10.1088/0957-4484/23/29/294003.

[48] Y. Yang, D. Ni, Y. Yao, Y. Zhong, Y. Ma, J. Yao, High photocatalytic activity of carbon doped TiO_2 prepared by fast combustion of organic capping ligands, RSC Adv. 5 (2015) 93635–93643. doi:10.1039/c5ra19058d.

[49] C. Di Valentin, G. Pacchioni, A. Selloni, Theory of carbon doping of titanium dioxide, Chem. Mater. 17 (2005) 6656–6665. doi:10.1021/cm051921h.

[50] K.S.W. Sing, D.H. Everett, R.A.W. Haul, L. Moscou, R.S. Pierotti, J. Rouquerol, T. Siemieniewska, Reporting physisorption data for gas/solid systems with special reference to the determination of surface area and porosity, Pure Appl. Chem. 57 (1985) 603–619. doi:10.1351/pac198557040603.

[51] K. Siwińska-Stefańska, A. Kubiak, A. Piasecki, J. Goscianska, G. Nowaczyk, S. Jurga, T. Jesionowski, TiO_2-ZnO binary oxide systems: Comprehensive characterization and tests of photocatalytic activity, Materials 11 (2018) 841. doi:10.3390/ma11050841.

[52] P. Shao, J. Tian, Z. Zhao, W. Shi, S. Gao, F. Cui, Amorphous TiO_2 doped with carbon for visible light photodegradation of rhodamine B and 4-chlorophenol, Appl. Surf. Sci. 324 (2015) 35–43. doi:10.1016/j.apsusc.2014.10.108.

[53] G. Goodman, Pentachlorophenol, in: R.I. Krieger, W.C. krieger (Eds.), Handbook of Pesticide Toxicology, Academic Press, 2001, 1480–1481.

[54] Agency for Toxic Substances and Disease Registry, Public Health Statement for Chlorophenols, 1990.

[55] C.C. Abnet, Carcinogenic Substances in Food : Mechanisms, Cancer Invest. 25 (2003) 189–196. doi:10.1080/07357900701208733

[56] Department of Health and Human Services, Public health service agency for toxic substances and disease registry, Agency for Toxic Substances and Disease Registry 1999.

[57] M. Goel, J.M. Chovelon, C. Ferronato, R. Bayard, T.R. Sreekrishnan, The remediation of wastewater containing 4-chlorophenol using integrated photocatalytic and biological treatment, J. Photochem. Photobiol. B Biol. 98 (2010) 1–6. doi:10.1016/j.jphotobiol.2009.09.006.

[58] H.J.R. F. Westmeier, Degradation of 4-chlorophenol in municipal wastewater by adsorptiv immobilized Aicaligenes sp. A 7-2, Appl. Microbiol. Biotechnol. 26 (1987) 78–83. doi:10.1007/978-81-322-2259-0.

[59] A. Kubiak, K. Siwińska-Ciesielczyk, Z. Bielan, A. Zielińska-Jurek, T. Jesionowski, Synthesis of highly crystalline photocatalysts based on TiO_2 and ZnO for the degradation of organic impurities under visible-light irradiation, Adsorption. 25 (2019) 309-325. doi:10.1007/s10450-019-00011-x.

[60] Y.T. Lin, C.H. Weng, Y.H. Lin, C.C. Shiesh, F.Y. Chen, Effect of C content and calcination temperature on the photocatalytic activity of C-doped TiO_2 catalyst, Sep. Purif. Technol. 116 (2013) 114–123. doi:10.1016/j.seppur.2013.05.018.

[61] D. Li, H. Haneda, N. Ohashi, S. Hishita, Y. Yoshikawa, Synthesis of nanosized nitrogen-containing MO_x-ZnO (M = W, V, Fe) composite powders by spray pyrolysis and their visible-light-driven photocatalysis in gas-phase acetaldehyde decomposition, Catal. Today. 93–95 (2004) 895–901. doi:10.1016/j.cattod.2004.06.099.

[62] C. Zhang, Y. Li, J. Li, Improved disinfection performance towards human adenoviruses using an efficient metal-free heterojunction in a vis-LED photocatalytic membrane

reactor: Operation analysis and optimization, Chem. Eng. J. 392 (2020). doi:10.1016/j.cej.2019.123687.

[63] J. Low, J. Yu, M. Jaroniec, S. Wageh, A.A. Al-Ghamdi, Heterojunction Photocatalysts, Adv. Mater. 29 (2017) 1601694. doi:10.1002/adma.201601694.

[64] A. Durán, J.M. Monteagudo, I. San Martín, Photocatalytic treatment of an industrial effluent using artificial and solar UV radiation: An operational cost study on a pilot plant scale, J. Environ. Manage. 98 (2012) 1–4. doi:10.1016/j.jenvman.2011.12.007.

[65] U. Stafford, K.A. Gray, P. V. Kamat, Radiolytic and TiO_2-assisted photocatalytic degradation of 4-chlorophenol. A comparative study, J. Phys. Chem. 98 (1994) 6343–6351. doi:10.1021/j100076a019.

[66] X. Li, J.W. Cubbage, T.A. Tetzlaff, W.S. Jenks, Photocatalytic degradation of 4-chlorophenol. 1. The hydroquinone pathway, J. Org. Chem. 64 (1999) 8509–8524. doi:10.1021/jo990820y.

[67] T. Lee, H.T. Bui, J. Yoo, M. Ra, S.H. Han, W. Kim, W. Kwon, Formation of TiO_2@Carbon core/shell nanocomposites from a single Mmlecular layer of aromatic compounds for photocatalytic hydrogen peroxide generation, ACS Appl. Mater. Interfaces. 11 (2019) 41196–41203. doi:10.1021/acsami.9b10015.

[68] Y. Zhang, Y. Li, H. Yu, K. Yu, H. Yu, Interfacial defective Ti^{3+} on Ti/TiO_2 as visible-light responsive sites with promoted charge transfer and photocatalytic performance, J. Mater. Sci. Technol. 106 (2022) 139–146. doi:10.1016/j.jmst.2021.06.081.

[69] Y. Xu, S. Wu, P. Wan, J. Sun, Z.D. Hood, Introducing Ti^{3+} defects based on lattice distortion for enhanced visible light photoreactivity in TiO_2 microspheres, RSC Adv. 7 (2017) 32461–32467. doi:10.1039/c7ra04885h.

[70] F.J.A. Villaluz, M.D.G. de Luna, J.I. Colades, S. Garcia-Segura, M.C. Lu, Removal of 4-chlorophenol by visible-light photocatalysis using ammonium iron(II) sulfate-doped

nano-titania, Process Saf. Environ. Prot. 125 (2019) 121–128. doi:10.1016/j.psep.2019.03.001.

[71] A.B. Lavand, Y.S. Malghe, Visible light photocatalytic degradation of 4-chlorophenol using C/ZnO/CdS nanocomposite, J. Saudi Chem. Soc. 19 (2015) 471–478. doi:10.1016/j.jscs.2015.07.001.

[72] H. Fu, G. Shang, S. Yang, T. Xu, Mechanistic study of visible-light-induced photodegradation of 4-chlorophenol by $TiO_{2-x}N_x$ with low nitrogen concentration, Int. J. Photoenergy. 2012 (2012). doi:10.1155/2012/759306.

[73] Z. Huang, Z. Chen, A. Qayum, X. Zhao, H. Xia, F. Lu, L. Hu, Enhanced photocatalytic degradation of 4-chlorophenol under visible light over carbon nitride nanosheets with carbon vacancies, Nanotechnology. 32 (2021). doi:10.1088/1361-6528/ac0eac.

[74] M. Hatori, C. Gronfier, R.N. Van Gelder, P.S. Bernstein, J. Carreras, S. Panda, F. Marks, D. Sliney, C.E. Hunt, T. Hirota, T. Furukawa, K. Tsubota, Global rise of potential health hazards caused by blue light-induced circadian disruption in modern aging societies, npj Aging Mech. Dis. 3 (2017) 5–7. doi:10.1038/s41514-017-0010-2.

[75] C. Casado, R. Timmers, A. Sergejevs, C.T. Clarke, D.W.E. Allsopp, C.R. Bowen, R. van Grieken, J. Marugán, Design and validation of a LED-based high intensity photocatalytic reactor for quantifying activity measurements, Chem. Eng. J. 327 (2017) 1043–1055. doi:10.1016/j.cej.2017.06.167.

[76] H. O'Neal Tugaoen, S. Garcia-Segura, K. Hristovski, P. Westerhoff, Compact light-emitting diode optical fiber immobilized TiO_2 reactor for photocatalytic water treatment, Sci. Total Environ. 613–614 (2018) 1331–1338. doi:10.1016/j.scitotenv.2017.09.242.

Figure captions

Fig. 1. The FTIR spectra of (a) reference TiO_2 and CTAB, (b) TiO_2-C nano-composite.

Fig. 2. The remission function, F(R), in UV-Vis of synthesized TiO_2-C nanocomposite and P25 sample.

Fig. 3. The TEM images of synthesized systems: (a) TiO_2; (b) TiO_2_300; (c) TiO_2_325; (d) TiO_2_350; (e) TiO_2_375; (f) TiO_2_400.

Fig. 4. The HR-TEM and FFT images for: (a) TiO_2_300; (b) TiO_2_325; (c) TiO_2_350; (d) TiO_2_375; (e) TiO_2_400.

Fig. 5. The XRD pattern (a) and Raman spectra (b) for TiO_2-C nanocomposite.

Fig. 6. EPR spectra of TiO_2 and the synthesized TiO_2-C nanostructures at RT (a), and for samples of TiO2_300 (b) and of TiO2_375 (c) at 83 K and 81 K, respectively.

Fig. 7. Nitrogen adsorption-desorption isotherms for the synthesized TiO_2-C nanocomposite.

Fig. 8. The results of photo-oxidation of 4-chlorophenol for TiO_2-C nanocomposite using: (a) 3500K LED, (b) 4500K LED, (c) 6500K LED, and (d) solar as light source.

Fig. 9. The proposed mechanism of 4-chlorophenol photodegradation of using TiO_2-C photocatalysts.

Fig. 10. Images from the thermal imaging camera for the 4500K LED: (a) 5 min and (b) 6 h after switching on

Table captions

Table 1. The results of elemental analysis, X-ray diffraction, low-temperature N_2 sorption, and diffuse reflectance spectroscopy for TiO_2-C nanocomposites.

Table 2. Comparison of 4-chlorophenol removal of other photocatalysts.

Adam Kubiak: Conceptualization, Methodology, Formal analysis, Investigation, Data curation, Writing - Original Draft; **Anna Grzegórska:** Formal analysis, Data Curation; **Elżbieta Gabała:** Formal analysis, Investigation; **Joanna Zembrzuska:** Formal analysis, Methodology, Data Curation; **Mirosław Szybowicz:** Formal analysis, Methodology, Data

Curation; **Hubert Fuks:** Formal analysis, Methodology, Data Curation, Writing - Review & Editing; **Anna Szymczyk:** Formal analysis, Methodology, Data Curation, Writing - Review & Editing; **Anna Zielińska-Jurek:** Formal analysis, Data Curation; **Teofil Jesionowski:** Writing - Review & Editing, Project administration, Funding acquisition; **Marek Sikorski:** Supervision, Writing - Review & Editing.

- we propose a facile surfactant-assisted synthesis of TiO_2-C nano-structures,
- we report the key impact of the LEDs color temperature on the photooxidation efficiency,
- commercial energy-saving LEDs are cheap alternatives to Xe- and Hg- light sources,
- tailor-made photocatalytic systems were proposed as a novel approach to photocatalysis.

Table 1. The results of elemental analysis, X-ray diffraction, low-temperature N_2 sorption, and diffuse reflectance spectroscopy for TiO_2-C nanocomposites.

Elemental analysis				Crystalline structure			BET surface area			Ban
N (%)	C (%)	H (%)	S (%)	Average crystallite size (nm)	Lattice parameters		A_{BET} (m^2/g)	V_p (cm^3/g)	S_p (Å)	
					a (Å)	c (Å)				
1.735(2)	6.844(1)	2.668(4)	0.358(6)	–	–	–	400	0.329	35	
0.268(5)	4.978(4)	0.748(1)	0.309(1)	11.1(2)	3.79382(3)	9.47371(1)	173	0.277	44	
0.250(8)	3.948(7)	0.689(0)	0.323(5)	11.3(1)	3.79340(4)	9.47127(6)	100	0.120	58	
0.083(3)	3.241(6)	0.365(1)	0.332(5)	11.8(4)	3.79267(9)	9.44272(6)	92	0.132	65	
0.083(1)	2.509(6)	0.247(9)	0.307(5)	12.8(7)	3.79031(6)	9.41299(1)	58	0.121	63	
0.055(6)	2.259(0)	0.168(6)	0.281(8)	14.2(8)	3.78974(1)	9.40186(4)	45	0.106	60	

Table 5. Comparison of 4-chlorophenol removal of other photocatalysts.

aterial	Degradation conditions

	Concentration	Amount of photocatalyst	Type of light source	Range wavenumber of the light source	Power of light source	Degradation efficiency
O_2_350	10 mg/dm^3	1 g/dm^3	6500K LED	400-750 nm	30 W	95% (in 3 h)
N/S-TiO_2	10 mg/dm^3	1 g/dm^3	blue-LED	450 nm	25 W	99% (in 3h)
nO/CdS	10 mg/dm^3	0.5 g/dm^3	fluorescent lamp	λ>420 nm	65 W	95% (in 2.5 h)
S−Cu_2S	10 mg/dm^3	1 g/dm^3	metal halide lamp	λ>420 nm	400 W	90% (in 5h)
O_{2-X}-N_x	10 mg/dm^3	0.5 g/dm^3	xenon lamp	λ>420 nm	500W	90% (in 5h)
-C_3N_4	10 mg/dm^3	1 g/dm^3	xenon lamp	λ>420 nm	300W	60% (in 2h)

(a)

Wavenumber (cm^{-1})	Vibration type	Functional group
750	stretching	≡Ti-O
1400	bending	C-H
1475	stretching	C-N
1620	–	physically adsorbed water
2850	stretching	C-H (methyl groups)
2900	stretching	C-H (methylene groups)
3400	stretching	-OH

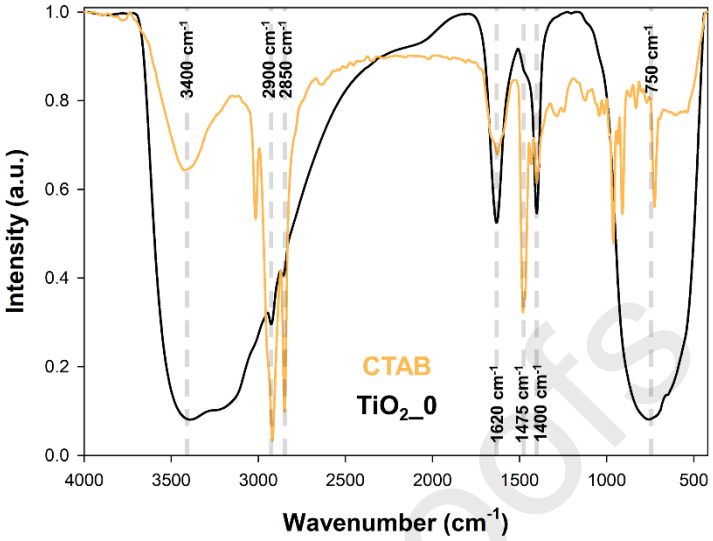

(b)

Wavenumber (cm^{-1})	Vibration type	Functional group
750	stretching	≡Ti-O
1400	bending	C-H
1620	–	physically adsorbed water
3400	stretching	-OH